Drag reduction of three-dimensional bodies by base-blowing with various gas densities

M. Lorite-Díez,[1] J. I. Jiménez-González,[1] L. Pastur,[2] O. Cadot,[3] and C. Martínez-Bazán[1]

[1] *Departamento de Ingeniería Mecánica y Minera. Universidad de Jaén. Campus de las Lagunillas, 23071, Jaén, Spain.*
[2] *IMSIA-ENSTA ParisTech, 828 Bd des Maréchaux F-91762 Palaiseau, France.*
[3] *School of Engineering, University of Liverpool, Liverpool L69 3GH, UK.*

(Dated: June 16, 2020)

The study reveals that injecting a light fluid of density ρ_b in the recirculating bubble of a bluff body at Re $\approx 6.4 \times 10^4$ has a greater drag reduction potential than blowing fluid of density greater than or equal to that of the free-stream, ρ. It is found that the maximum drag reduction scales as $(\rho_b/\rho)^{-\frac{1}{6}}$. This power law combines the ability of the recirculating bubble to diffuse the injected momentum and the effectiveness of the injection to increase the recirculating bubble length.

Since the seminal work of Wood [1], it is well known that injecting fluid in the recirculating bubble at the rear of two dimensional bluff bodies reduces the aerodynamic drag. The drag reduction mechanism, later confirmed by Bearman [2], is associated with a growth of the recirculating flow known to be intimately related to the base suction C_B (Roshko [3]) defined as minus the mean pressure at the base of the body. The technique is efficient to reduce drag of high speed projectiles and most of the fundamental research has focused on compressible flows with transonic and supersonic regimes of axisymmetric bodies [4, 5]. Although the technique is also considered to reduce aerodynamics drag in all transportation industries implying blunt base bluff bodies, or to suppress bluff bodies vortex-induced vibrations [6], there is only few fundamental investigations for three-dimensional bodies in incompressible flows in the literature [7–9].

The authors recently proposed a budget model [9] that establishes the relationship between the recirculating bubble length and the volumetric injection flow rate. The model is inspired by the mechanics of the formation region of vortices behind bluff bodies due to Gerrard [10]. Results are obtained from an experiment with slits injection at the body base, likely to be implemented in practice since they also work as passive drag reduction devices [11]. Lorite-Díez *et al.* [9] distinguish two different regimes, namely a *mass* regime and a *momentum* regime. The *mass* regime takes place at small injection flow rate, in which the added fluid is considered as a passive scalar, i.e. as a diffusive species that is present in such low concentration that it has no dynamical effect on the fluid motion itself [12, 13]. In this case, the injected fluid inflates the recirculating bubble, whose equilibrium size results from the extra leakages through the mixing layers introduced by the growth of the recirculating bubble. These leakages are shown to be in agreement with the entrainment velocity measured for isolated turbulent mixing layers [9]. This mass regime is associated with drag reduction and usually referred to as base bleed effects in the literature [1, 2]. Besides, at large injection flow rate, a new regime, called the *momentum* regime in Lorite-Díez *et al.* [9], is characterized by a strong flow modification associated with a bubble shortening. In this case, the injected fluid is directly evacuated from the recirculating bubble by its own momentum and the bubble size equilibrium results from additional leakages in the mixing layers. The momentum regime is associated with a drag increase, and the transition between the mass and the momentum regimes is then easily defined as the injection flow rate producing the largest bubble length or equivalently the lowest drag.

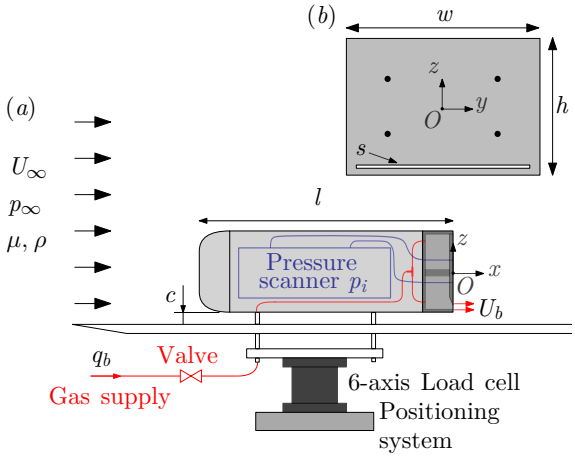

Figure 1. (a) Sketch of the experimental set-up. (b) Base of the bluff body depicting the pressure taps location (with black dots) and the blowing slit of surface s placed and the bottom of the body base.

The aim of the present contribution is to include density effect for this drag reduction mechanism, known to modify the stability properties of wake [14]. We will show in this rapid communication that the transition from the mass to the momentum regime, where the lowest drag is observed, is governed by the ability of the recirculating bubble to diffuse the injected momentum. The key result is that a lighter gas allows to increase the injection velocity for a given momentum, extending the mass regime to a larger maximum injection rate, and thus producing a longer bubble along with a lower drag. However, the bubble growth efficiency with the injection rate is found to be reduced with a lighter gas.

The experimental set-up is identical to that of Lorite-

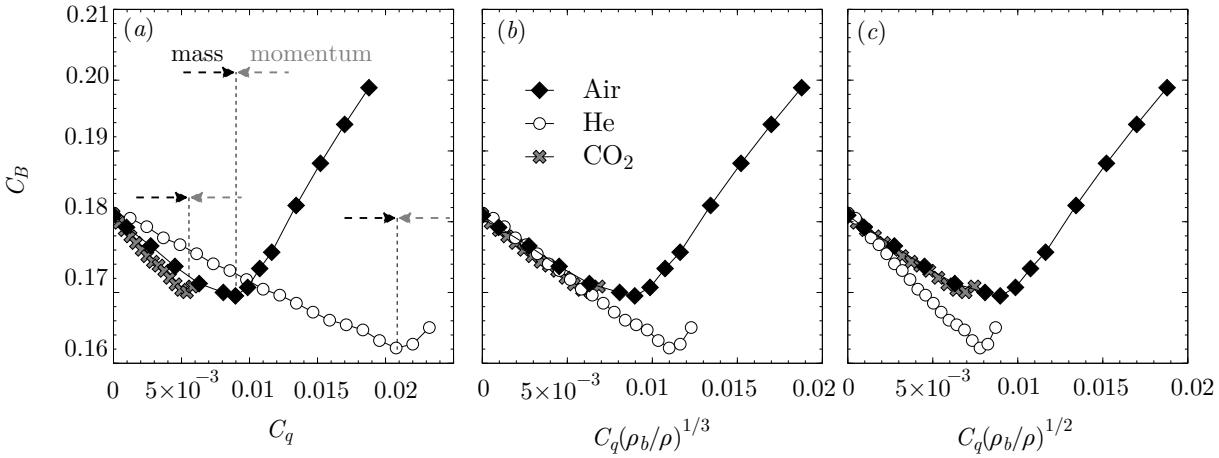

Figure 2. Base suction coefficient C_B versus the volumetric flow rate coefficient C_q (a), and the scaled coefficients $C_q(\rho_b/\rho)^\alpha$ (b and c) as power laws of the density ratio. Vertical dashed lines in (a) indicate the transition from the mass to the momentum regimes for each gas as described in Lorite-Díez *et al.* [9]

Díez *et al.* [9]. Briefly, the body shown in Fig. 1 has dimensions $l = 291$ mm, $w = 97.25$ mm and $h = 72$ mm. It is supported by four cylindrical rods of 7.5 mm in diameter with a ground clearance $c = 20$ mm $= 0.278h$. It is placed inside a 390 mm $\times$ 390 mm test section of an Eiffel-type wind tunnel. The velocity of the uniform stream is $U_\infty = 13.3$ m.s^{-1} giving a Reynolds number Re $= \rho U_\infty h/\mu \approx 6.4 \times 10^4$, where μ is the dynamic viscosity and ρ the density of air. The turbulent intensity is below 0.5% and the velocity homogeneity over the test section better than 0.3% [see 15, for further details]. Blowing of Air, Carbon Dioxide and Helium with density ρ_b is carried out through a single narrow horizontal slit placed at the bottom of the body base, having dimensions 87.25 mm $\times$ 2 mm and a surface $s = 0.025\,hw$ (see Fig. 1b). Their density ratios are ρ_b/ρ =1, 1.648 and 0.148 for Air, CO_2 and He respectively. As sketched in Fig. 1(a), the slit is connected to an internal cavity, pressurised by four pneumatic tubes at each corner which are joined to a single pneumatic injection tube. This injection tube includes an Aalborg digital flow meter specifically calibrated for each gas, a precision valve and a pressure regulator to ensure a constant volumetric flow rate q_b [see 9, for details]. The volumetric flow rate blowing coefficient is defined as

$$C_q = q_b/(hwU_\infty). \tag{1}$$

In the following, quantities with an asterisk superscript are made dimensionless using h and U_∞.

Pressure measurements are performed through four different pressure taps, placed at $(y^*, z^*) = (\pm 0.3, \pm 0.2)$ as indicated in Fig. 1, and connected to a Scanivalve ZOC22 pressure scanner working at a sampling rate of 100 Hz per channel. As established by Grandemange *et al.* [16], such an arrangement can be considered as the relevant minimal set of measurements to assess the mean base suction coefficient [3, 17] defined as

$$C_B = -\frac{1}{4}\Sigma_{i=1}^{4}\frac{\overline{p_i} - p_\infty}{\rho U_\infty^2/2}, \tag{2}$$

where $\overline{p_i}$ denotes the mean pressure at the location i and p_∞ is the reference static pressure at the inlet of the test section. The duration for the averaging is 60 s and the uncertainty in the base suction coefficient is estimated to be ± 0.002.

The drag force exerted on the body is measured with a multi-axial load cell (model AMTI-MC3A-100lb) as shown in Fig. 1(a) and acquired at a sampling rate of 1 kHz. The uncertainty of the measurements is estimated to be 0.002 N. Since we are interested in the mean drag without any contribution produced by the blowing system itself, we subtract to the mean force obtained for a given base blowing and wind speed, $\overline{f_d(C_q, U_\infty)}$, the mean force produced by the blowing alone (without wind flow), $\overline{f_d(C_q, U_\infty = 0)}$. The mean value then reads

$$\tilde{C}_d = \frac{\overline{f_d(C_q, U_\infty)} - \overline{f_d(C_q, U_\infty = 0)}}{hw\rho U_\infty^2/2}. \tag{3}$$

Hence, $\tilde{C}_d$ is the aerodynamic drag coefficient when the blowing jet effects are removed. The duration for the averaging is 30 s, being the experimental protocol to obtain accurate values fully described in [9].

The near wake velocity fields are measured using Particle Image Velocimetry (PIV) in the two perpendicular planes $y^* = 0$ and $z^* = 0$. The PIV system uses a dual pulse laser (Nd:YAG, 2 x 135mJ, 4ns) synchronized with a FlowSense EO, 4 Mpx, CCD camera. Statistics are performed over 500 velocity fields sampled at 10 Hz. Velocities were computed from an interrogation window of 16 pixels $\times$ 16 pixels with an overlap of 50%, resulting in a spatial resolution of 1% of the body's height. Further details about the PIV procedure can be

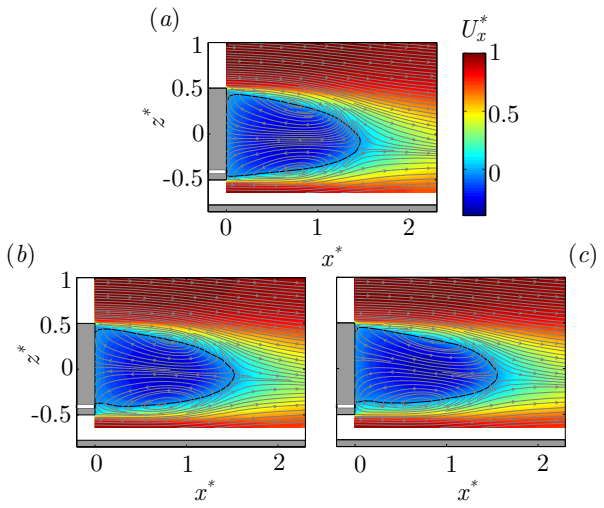

Figure 3. Averaged streamwise velocity U_x^* contours at $y^* = 0$ plane along with averaged flow streamlines (grey lines). The black continuous line denotes the values $U_x^* = 0$. Case with no injection (a), cases with air (b) at $C_q^{\mathrm{Opt}} = 0.008$ and Helium (c) at $C_q^{\mathrm{Opt}} = 0.021$. The blowing slit is indicated with the white band.

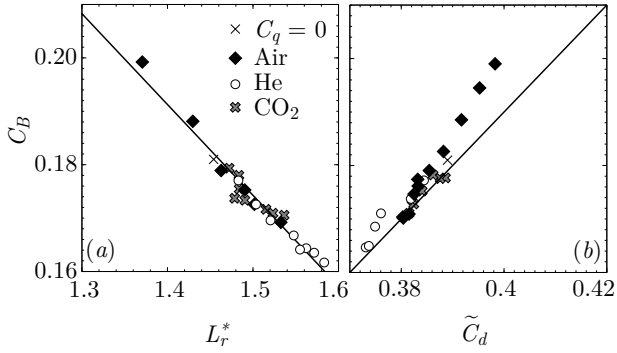

Figure 4. Recirculation length L_r^* (a) and drag coefficient $\tilde{C}_d$ (b) vs. base suction C_B for the 3 gases and the case with no blowing.

also found in [9].

The evolution of the base suction C_B with the volumetric flow rate coefficient is shown in Fig. 2(a) for the three injected gases. They all present a constant slope at small C_q over the mass regime range. The effect of the gas density is clearly observable from these curves: the heavier the gas, the steeper the slope and the shorter the mass regime. Figure 2(b) suggests that a simple power law scaling of density ratio to describe the mass regime is

$$C_B = C_B(C_q = 0) - a\ (\rho_b/\rho)^{\frac{1}{3}}\ C_q, \qquad (4)$$

with $a \approx 1.67$. Similarly, Fig. 2(c) suggests that a power law scaling to describe the optimal blowing coefficient for which the minimum base suction is reached is

$$C_q^{\mathrm{Opt}} = b\ (\rho_b/\rho)^{-\frac{1}{2}}\,, \qquad (5)$$

where $b \approx 8 \times 10^{-3}$. Note that, the lightest gas leads to the best reduction in base suction (with 10.6% for Helium, 6.3% for Air and 5.9% for CO_2) but with less efficiency since the optimal drag reduction is reached with a slope that decreases with the gas density as $(\rho_b/\rho)^{\frac{1}{3}}$ (see Eq. 4) and, thus, it is achieved at higher values of C_q. The main change in the flow with base blowing is the growth of the recirculating bubble [1, 2, 9], as illustrated with the mean velocity fields shown in Fig. 3. The bubble is clearly identifiable with the streamlines pattern and corresponds to the low speed region in blue containing two counter rotating vortices. The black line represents the loci of $U_x^* = 0$ and encloses by definition the whole feedback flow (i.e. $U_x^* < 0$). The characteristic size of the bubble is defined as the distance from the base to the furthest location where the mean streamwise velocity U_x^* is equal to zero. We can see that bubbles with optimal base blowing in Fig. 3(b,c) are elongated compared to Fig. 3(a) and the longest bubble is achieved with Helium which also corresponds to the largest base suction reduction. As in Lorite-Díez *et al.* [9] we define the bubble size L_r^* as the average of the characteristic sizes (as defined from above) measured in the two perpendicular planes $y^* = 0$ and $z^* = 0$. It is plotted versus the base suction in Fig. 4(a) and shows a very good correlation independently of the gas used. It reminds the work of Bearman [2] about a 2D blunt cylinder who achieved a unique relationship using either iso-density base bleeding or splitter plate. This universal behavior confirms the relevance of the inviscid cavity models (see the review by [18]) for blunt bodies at large Reynolds number. These models establish a general behavior of base suction evolving as positive power laws of the inverse of the cavity length. Physically, the low base pressure is produced by the inviscid flow curvature around the cavity. For viscous wake flows at large Reynolds number, this trend still remains with the recirculating bubble playing the role of the cavity [3]. In our case, the variations of the bubble length L_r^* are small compared to the reference value of $L_r^* = 1.45$ which linearizes the power law to the affine law as observed in Fig. 4(a).

The relationship between the drag coefficient and the base suction is straightforward since the base suction C_B is the rear part contribution of the pressure drag. The drag coefficient thus reads $\tilde{C}_d = C_B + C_F + C_f$, where C_F accounts for the forebody pressure integration and C_f for the wall friction. With base blowing, neither the forebody nor the friction contributions are supposed to change significantly, thus leading to identical variations for base suction and drag coefficient, $\Delta\tilde{C}_d \approx \Delta C_B$. The discrepancy to the slope 1 observed for larger drag (i.e. smaller bubble length obtained with large blowing) in Fig. 4(b) is likely to be due to the blowing jet effects that cannot be completely removed using Eq. (3) because of the interaction of the blowing jet with the flow. In

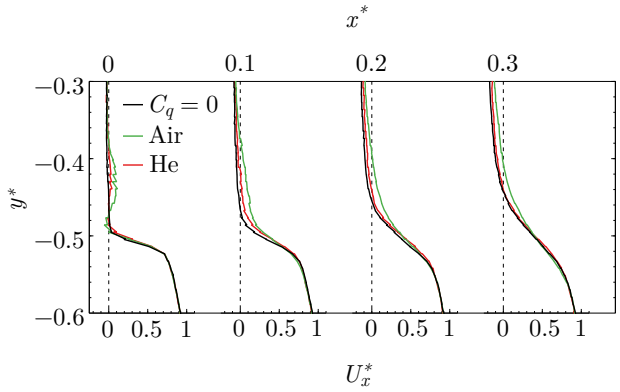

Figure 5. Mean velocity profiles of the mixing layer that develops from the bottom edge of the base. Time averaged velocity profiles, U_x^* at several streamwise locations for the non-blowing case and two blowing flow rates employing He and Air which produce the same recirculation region length, $L_r^* = 1.54$.

addition, the low velocity of the incoming flow $U_\infty = 13.3$ m.s^{-1} makes our data more scattered due to the force balance limitation than those presented in Lorite-Díez *et al.* [9], working at $U_\infty = 20$ m.s^{-1}. Overall, the drag coefficient evolves monotonously with the base suction as expected.

The bubble growth model in the *mass regime* [9] results from the equilibrium between mass fluxes feeding and emptying the recirculating region as introduced by [10]. Based on simple arguments they obtain

$$L_r^* = L_{r0}^* + \frac{w}{V_E^* \ell} C_q, \tag{6}$$

where $\ell = 2h + 2w$ is the peripheral length of the mixing layers bounding the recirculation bubble.

Figure 5 shows the mixing layer that develops at the bottom of the base, from the $z^* = -0.5$, $x^* = 0$ edge. The case with no injection is showed as a reference, the case with air injection at $C_q = 0.008$ corresponds to the end of the mass regime and with Helium injection at $C_q = 0.014$ approximately corresponds to the middle of the mass regime. These two cases of injection have been chosen because they lead to the same bubble length, $L_r^* = 1.54$ and then to the same base suction. The velocity profiles indicate that the Helium injection has less effect on the mixing layer development than Air injection has. The weak tendency is a slightly steeper gradient with Helium than with Air that is consistent with a decrease in the entrainment velocity. This observation is in agreement with the density effects reported on turbulent mixing layers by Brown and Roshko [19] and it is also expected with linear stability analysis [7]. Within the framework of the model in Eq. (6), this flow modification fails to explain the weaker efficiency using lower density fluid (i.e. slope approximated by Eq. 4) since the weaker the efficiency means the larger the entrainment velocity. It is then better to consider the injected fluid as a passive scalar and we suggest that the pressure field dynamics inside and at the closure of the recirculation bubble is responsible for the density effect through the horsehoe vortical structures [20–22] connecting the interior of the separation and the wake. As low density fluid is attracted and high density fluid repelled by low pressure associated with the vortical structure we speculate that low density fluid is preferentially evacuated from the bubble while high density fluid is likely to remain.

The transition between the mass and momentum regime leading to optimal drag reduction was found in Lorite-Díez *et al.* [9], by changing the area of injection, to depend on the global flow rate injected in the bubble, and not on the local momentum injection. This result is generalised including density effect with Eq. (5). It is interpreted as the maximum injected momentum flux, $\rho_b u_b^{\rm Opt} s u_b^{\rm Opt}$, which can be efficiently diffused by the flow in the separated area such that the injected fluid behaves as a passive scalar (the *mass regime* condition). The momentum diffusion is taken into account with a dilution factor $s/(hw)$ such that the maximum injected momentum flux reads

$$\Pi = \rho_b u_b^{\rm Opt} s u_b^{\rm Opt} \times \frac{s}{hw} = \frac{\rho_b}{hw} \left(q_b^{\rm Opt}\right)^2. \tag{7}$$

In dimensionless unit, $\Pi/(\rho h w U_\infty^2) = (\rho_b/\rho)(C_q^{\rm Opt})^2 = b^2$ as found experimentally in Eq. (5). Hence, using the measured value of b, the maximum momentum flux born by the bubble in the mass regime is $\Pi \approx 6.4 \times 10^{-5} \rho h w U_\infty^2$. Finally, taking into account the scaling laws in Eqs.(4) and (5), the maximum drag variation that can be achieved is given by

$$\Delta C_B^{\rm Opt} = -a\, b\, (\rho_b/\rho)^{-\frac{1}{6}} \approx -1.33 \times 10^{-2} (\rho_b/\rho)^{-\frac{1}{6}}. \tag{8}$$

ACKNOWLEDGMENTS

This work has been partially supported by the Spanish MINECO and European Funds under projects DPI2017-89746- R and DPI2017-88201-C3-2-R. Moreover, J.I.J.G. and M.L.D want to thank the Spanish MECD for the financial support provided under José Castillejo grant CAS18/00379 and Fellowship FPU 014/02945 respectively.

[1] C. J. Wood, Aeronaut. J. **68**, 477 (1964).
[2] P. W. Bearman, Aeronaut. Quart. **18**, 207 (1967).
[3] A. Roshko, J. Wind Eng. Ind. Aerodyn. **49**, 79 (1993).
[4] M. Tanner, Prog. Aerosp. Sci. **16**, 369 (1975).

[5] P. R. Viswanath, Prog. Aerosp. Sci. **32**, 79 (1996).
[6] S. Dong, G. S. Triantafyllou, and G. E. Karniadakis, Phys. Rev. Lett. **100**, 204501 (2008).
[7] A. Sevilla and C. Martínez-Bazán, Phys. Fluids **16**, 3460 (2004).
[8] P. Bohorquez, E. Sanmiguel-Rojas, A. Sevilla, J. I. Jiménez-González, and C. Martínez-Bazán, J. Fluid Mech. **676**, 110 (2011).
[9] M. Lorite-Díez, J. I. Jiménez-González, L. Pastur, C. Martínez-Bazán, and O. Cadot, J. Fluid Mech. **883**, A53 (2020).
[10] J. H. Gerrard, J. Fluid Mech. **25**, 401 (1966).
[11] J. M. García de la Cruz, A. R. Oxlade, and J. F. Morrison, Phys. Rev. Fluids **2**, 043905 (2017).
[12] Z. Warhaft, Annu. Rev. Fluid Mech. **32**, 203 (2000).
[13] A. Attili and F. Bisetti, Phys. Rev. E **88**, 033013 (2013).
[14] A. Sevilla and C. Martínez-Bazán, Phys. Fluids **18**, 098102 (2006).
[15] O. Cadot, A. Evrard, and L. Pastur, Phys. Rev. E **91**, 063005 (2015).
[16] M. Grandemange, M. Gohlke, and O. Cadot, Phys. Fluids **25**, 095103 (2013).
[17] C. Apelt and G. West, J. Fluid Mech. **71**, 145 (1975).
[18] T. Y. T. Wu, Annu. Rev. Fluid Mech. **4**, 243 (1972).
[19] G. L. Brown and A. Roshko, J. Fluid Mech. **64**, 775 (1974).
[20] A. Evrard, O. Cadot, V. Herbert, D. Ricot, R. Vigneron, and J. Délery, J. Fluids Struct. **61**, 99 (2016).
[21] H. J. Schmidt, R. Woszidlo, C. N. Nayeri, and O. Paschereit, Exp. Fluids **59**, 107 (2018).
[22] G. Pavia, M. A. Passmore, M. Varney, and G. Hodgson, J. Fluid Mech. **888**, A33 (2020).